AAEC/E403

AUSTRALIAN ATOMIC ENERGY COMMISSION

RESEARCH ESTABLISHMENT

LUCAS HEIGHTS

VALENCE NEUTRON CAPTURE IN ^{54}Fe**

by

B.J. ALLEN
A.R. de L. MUSGROVE
J.W. BOLDEMAN
*R.L. MACKLIN

**Research sponsored in part by ERDA under contract with Union Carbide Corporation

*Oak Ridge National Laboratory, Oak Ridge, Tenn. USA

February 1977
ISBN 0 642 99770 5

AUSTRALIAN ATOMIC ENERGY COMMISSION
RESEARCH ESTABLISHMENT
LUCAS HEIGHTS

VALENCE NEUTRON CAPTURE IN ^{54}Fe[†]

by

B.J. ALLEN
A.R. de L. MUSGROVE
J.W. BOLDEMAN
*R.L. MACKLIN

ABSTRACT

The neutron capture cross section of ^{54}Fe has been measured with 0.2 per cent energy resolution from 2.5 to 500 keV. A large and significant correlation is observed between the s-wave reduced neutron widths and the corresponding total radiative widths. The valence model readily accounts for this correlation as well as a large fraction of the s-wave radiative widths.

[†]Research sponsored in part by ERDA under contract to Union Carbide Corporation.

* Oak Ridge National Laboratory, Oak Ridge, Tenn. USA.

National Library of Australia card number and ISBN 0 642 99770 5

The following descriptors have been selected from the INIS Thesaurus to describe the subject content of this report for information retrieval purposes. For further details please refer to IAEA-INIS-12 (INIS: Manual for Indexing) and IAEA-INIS-13 (INIS: Thesaurus) published in Vienna by the International Atomic Energy Agency.

CAPTURE; CORRELATIONS; CROSS SECTIONS; DATA; GAMMA SPECTRA; IRON 54 TARGET; keV RANGE; LEVEL WIDTHS; NEUTRON REACTIONS; RESONANCE; S WAVES; VALENCE

CONTENTS

1. INTRODUCTION

Non-statistical processes are prevalent in the $40 < A < 70$ region where the 3s neutron orbital is just unbound. Low lying states have dominant 2p single particle character and E1 transitions following s-wave capture are predicted to be strong by the valence model [Lynn 1968]. Correlations between the reduced neutron widths and radiative widths of s-wave resonances have been observed [Block *et al.* 1971, Musgrove *et al.* 1976, Allen *et al.* 1976a,b], and resonance γ-ray spectra are dominated by strong transitions to the 2p final states [Bird *et al.* 1973].

However, the valence model has not been able to account for the observed radiative widths and γ-ray spectra and a further 2p-1h process has been proposed in Sc [Allen *et al.* 1976c] and ^{56}Fe [Allen *et al.* 1976a] to account for the data. Since ^{54}Fe resonances have some of the largest neutron widths in this mass region, the valence process might be expected to dominate the capture mechanism. To test this hypothesis, high resolution capture cross section measurements have been made and the results correlated with the recent total cross section data obtained by Pandy *et al.* [1975].

These results also satisfy, in part, reactor data needs listed in WRENDA 75. Resonance and cross section data have already been published for ^{56}Fe [Allen *et al.* 1976a] and measurements on ^{57}Fe have been completed.

2. MEASUREMENTS

The capture cross section measurements were made at the 40 metre station of the Oak Ridge Electron Linear Accelerator. Capture γ-rays were detected by two non-hydrogenous liquid scintillators [Macklin & Allen 1971, Macklin *et al.* 1971]. Events were weighted according to the measured pulse height to achieve a detector response proportional to the total energy of the capture reaction. A 0.5 mm thick ^{6}Li glass scintillator, 0.5 m upstream from the capture detectors, operated as a neutron monitor in the transmission mode [Macklin *et al.* 1971]. The ^{6}Li(n,α) cross section and efficiency perturbation caused by the glass constituents have been parameterised [Macklin *et al.* 1975].

The absolute efficiency of the capture detectors was determined by the saturated resonance method for the 4.9 eV resonance in gold. The overall detector efficiency has been found stable to 1.7 per cent (standard deviation) during repeated measurements at 4.9 eV over several months. The dominant error in the absolute normalisation, therefore, becomes that of the ^{6}Li(n,α) cross section, which varies from less than 2 per cent below 100 keV, 5 per cent below 300 keV, increasing to 10 per cent at 500 keV

[Allen *et al.* 1973].

Thin and thick sample measurements were made to minimise self-shielding and multiple-scattering corrections at low energies, and to obtain accurate statistics for energies up to 500 keV. Target thicknesses and ^{54}Fe isotopic abundances were 0.0020 atom b^{-1}, 98.80% and 0.0197 atom b^{-1}, 97.59% respectively.

3. ANALYSIS

The capture data were analysed using a modified version of the ORNL/RPI Monte Carlo code [Sullivan *et al.* 1969]. Breit-Wigner single-level theory was used to generate capture and total cross sections, and the observed capture areas were fitted by an iterative process after subtraction of the multiple scattering component. The thin sample capture area

$$A_\gamma = 2\pi^2 \lambda^2 g \Gamma_\gamma \Gamma_n / \Gamma$$

is obtained from the area fit. When $\Gamma_n > 0.2\ \Gamma_R$, where Γ_R is the experimental resolution, a shape fit can yield the neutron width Γ_n, and A_γ therefore provides an estimate of $g\Gamma_\gamma$. In the ^{54}Fe data, statistical errors are normally $\lesssim$5 per cent and for resonances with large neutron widths, uncertainties in the linear background estimate and corrections for overlapping resonances dominate. Representative samples of the capture data are given in Figure 1.

A prompt background correction is also made to account for the sensitivity of the capture detectors to resonance scattered neutrons. For most resonances, this correction is negligible but, when $\Gamma_\gamma/\Gamma_n \lesssim 10^{-4}$, the correction ($k\Gamma_n$) to the radiative width becomes substantial. Estimates of the correction factor have been obtained for resonances between 27 and 440 keV and the energy dependence has been investigated using C and ^{208}Pb scattering samples [Allen *et al.* 1973]. The correction at 7.7 keV, derived from a 1/v dependence normalised at 27 keV [Allen *et al.* 1976a], is consistent with the estimated radiative width obtained by extrapolation from the thermal capture cross section [Mughabghab 1974].

Asymmetric resonances were observed at 130, 148 and 174 keV after subtraction of the multiple-scattering component (38%, 17%, 7% respectively, of the primary yields). For the first two resonances this asymmetry is unlikely to result from the prompt, resonance scattered background, and could be indicative of interference effects. However, if the neutron widths are in error, then oversubtraction of the multiple scattering yield can

also result in asymmetry.

4. RESULTS

Parameters of resonances analysed up to 500 keV are given in Table 1, together with the capture results of Hockenbury *et al.* [1969] and Beer & Spencer [1975]. S-wave assignments are taken from Pandy *et al.* [1975] and d-wave assignments are deduced from the low values of $g\Gamma_n$ obtained from the area analysis. Excellent agreement in energy (to better than 0.1%) is found between the capture and total cross section data, but many more resonances are detected in capture. Neutron widths measured by Pandy *et al.* [1975] are given in Table 1, and these values have generally been used in the capture analysis. Where these widths are inconsistent with the capture data, both neutron widths are tabulated. Above 200 keV, a neutron width of 100 eV is used for self-shielding corrections unless otherwise specified.

Below 100 keV, neutron widths and spins were adjusted to yield comparable $g\Gamma_\gamma\Gamma_n/\Gamma$ values for both thin and thick sample measurements. The resonance parameter set is therefore consistent, but not necessarily unique. Consequently, neutron widths and spins are given as probable values only in Table 1.

The $\ell>0$ level density (Figure 2) increases slowly above 200 keV as d-wave resonances are detected with $\Gamma_n >> \Gamma_\gamma$. Above 300 keV, the level density decreases, indicating that resonances with lower values of $g\Gamma_\gamma$ are missed. Above 100 keV, $g\Gamma_\gamma\Gamma_n/\Gamma$ values (Figure 3) show an increasing trend with neutron energy. This result reflects the increase in d-wave neutron widths, such that $\Gamma_n > \Gamma_\gamma$, and the larger g values and radiative widths for these resonances.

Below 100 keV, unassigned resonances are assumed to be p-wave with $\Gamma_n \geq \Gamma_\gamma$. This assumption is suggested by the cutoff of $g\Gamma_\gamma\Gamma_n/\Gamma$ values at ~0.2 eV, and requires the p-wave strength function to be greater than $\sim 0.2 \times 10^{-4}$. The average radiative width of these resonances (assuming $\bar{g} = 1.67$) is 0.46 eV, a value which provides an excellent fit to the average capture cross section (Figure 4).

Above 200 keV, the d-wave component is calculated to dominate the capture cross section, and the average $\ell>0$ radiative width (assuming $\bar{g} = 2.6$) is 1.2 eV after a correction for p-wave resonances. This value is assumed to be representative of the d-wave population and provides a good fit to the average cross section above 200 keV.

Average resonance parameters are summarised in Table 2. Errors given for $\bar{\Gamma}_\gamma(p)$ and $\bar{\Gamma}_\gamma(d)$ are indicative of the uncertainty which exists in the above analysis.

Average capture cross sections are given in Table 3, together with the resonance component of the resonance integral above 2.5 keV ($\Sigma A_\gamma/E$), and the 30 keV Maxwellian averaged capture cross section ($\langle\sigma\cdot v\rangle/v_T$).

5. VALENCE MODEL

The valence radiative widths for E1 transitions from s-wave resonances to the $p_{1/2}$, $p_{3/2}$ final states are given in Table 4, together with the relevant s-wave data. The widths were calculated using the optical model approach [Lane & Mughabghab 1974, Barrett & Terasawa 1975]. Partial valence widths are given by

$$\Gamma^V_{\gamma\lambda\mu} = q_{\lambda\mu}(E_\lambda) \cdot E_\gamma^3 \cdot (Z/A)^2 \cdot S_\mu \cdot \Gamma^0_{\lambda n} \quad ,$$

and

$$\Gamma^V_{\lambda\gamma} = Q_\lambda(E_\lambda) \cdot \Gamma^0_{\lambda n} \quad ,$$

where $q_{\lambda\mu}$ denotes the dipole radial integral and geometric factors evaluated using Moldauer's optical model parameters which were adjusted to give the experimental, single particle centroid binding energies. The centroid energies and the spectroscopic factors S_μ, are taken from Kocher & Haeberli [1972] - see Table 4. Since q_λ is strongly energy dependent [Allen *et al.* 1976c], the valence width was evaluated at each resonance.

The calculated valence widths are compared with the measured radiative widths in Figure 5(a) as a function of energy, and account for large fractions of the observed widths of most resonances. The data are also consistent with the predicted energy dependence of the valence component. Without this dependence, the valence widths of resonances at 414 and 433 keV would be 8-10 eV, and several times larger than the measured values. The correlation between the calculated and observed widths is

$$\rho_v(\Gamma^V_\gamma, \Gamma_\gamma) = 0.93^{+0.07}_{-0.23},$$

where the error is the standard deviation of a zero correlation distribution calculated for the appropriate sample size. This result is similar to the initial state correlation of $\rho_I(\Gamma^0_n, \Gamma_\gamma) \approx 0.94$.

Further confirmation of the dominant role of the valence process is found in the thermal capture γ-ray spectrum. The thermal capture cross section of 2.3 barn is much larger than the estimated direct capture cross section, and is attributed to the 7.6 keV resonance [Mughabghab 1974]. Our value for the radiative width of this resonance is fully consistent with this interpretation, and calculated partial valence widths are in excellent agreement with the measured values (Table 5). The $\ell_n = 1$ final state correlation is $\rho_F(\Gamma^V_{\gamma\mu}, \Gamma_{\gamma\mu}) = 0.94^{+0.06}_{-0.39}$, reflecting the dominance of valence transitions to the $^3/_2^-$ ground state and $^1/_2^-$ first excited state.

Average γ-ray spectra [Bird *et al.* 1976] are available at 30 keV, but are not representative of s-wave capture. Nevertheless, these spectra also show strong transitions to the single particle final states, including the $^5/_2^-$ second excited state. Further measurements of γ-ray spectra from s-wave resonances are needed to confirm the dominant role of the valence capture mechanism.

The valence model is seen to account for both initial and final state correlations, and a large fraction of the partial and total radiative widths. This result is outstanding for the A=40-70 mass region where initial state correlations of less than 0.5 have been frequently observed together with valence magnitudes which are often much less than the observed widths.

In ^{56}Fe, evidence [Allen *et al.* 1976a] was found for a substantial uncorrelated component in the radiative widths. It is probable that this component is still present in ^{54}Fe, but its effect is diminished because of the valence component which is six times larger in ^{54}Fe than ^{56}Fe. The increased valence strength arises from the larger single particle binding energies and the s-wave strength function in ^{54}Fe.

6. REFERENCES

Allen, B.J., Macklin, R.L., Winters, R.R. & Fu, C.Y. [1973] - *Phys. Rev.*, C8:1504.

Allen, B.J., Musgrove, A.R. de L., Boldeman, J.W., Kenny, M.J. & Macklin, R.L. [1976a] - *Nucl. Phys.*, A269:408.

Allen, B.J., Boldeman, J.W., Musgrove, A.R. de L. & Macklin, R.L. [1976b] - AAEC/E (in preparation).

Allen, B.J., Kenny, M.J., Barrett, R.F. & Bray, K.H. [1976c] - *Phys. Lett.*, 61B:161.

Arnell, S.E. [1967] - Cited in Nuclear Data 3:515.

Barrett, R.F. & Terasawa, T. [1975] - *Nucl. Phys.*, A240:445

Beer, H. & Spencer, R.R. [1975] - *Nucl. Phys.*, A240:29.

Bird, J.R., Allen, B.J., Bergqvist, I. & Biggerstaff, J.A. [1973] - *Nuclear Data Tables*, 11:434.

Block, R.C., Steiglitz, R.G. & Hockenbury, R.W. [1971] - Proc. 3rd Conf. on Neutron Cross Sections & Technology, Knoxville, CONF-710701, 889.

Hockenbury, R.W., Bartolome, Z.M., Tatarczak, J.R., Moyer, W.R. & Block, R.C. [1969] - *Phys. Rev.*, 4. 178:1746.

Kenny, M.J., Allen, B.J., Musgrove, A.R. de L., Macklin, R.L. & Halperin, J. [1976] - AAEC/E400.

Kocher, D.C. & Haeberli, W. [1972] - *Nucl. Phys.*, A196:225.

Lane, A.M. & Mughabghab, S.F. [1974] - *Phys. Rev.*, C10:414.

Lynn, J.E. [1968] - Theory of Neutron Resonance Reactions Clarendon Press, Oxford.

Macklin, R.L., Allen, B.J. [1971] - *Nucl. Instrum. Methods*, 91:565.

Macklin, R.L., Hill, N.W. & Allen, B.J. [1971] - *Nucl. Instrum. Methods.*, 96:509.

Macklin, R.L., Halperin, J. & Winters, R.R. [1975] - *Phys. Rev.*, C11:1270.

Mughabghab, S.F. [1974] - Proc. 1st Symp. on Neutron Capture Gamma Ray Spectroscopy, Petten p.53.

Musgrove, A.R. de L., Allen, B.J., Boldeman, J.W., Chan, D.M.H. & Macklin, R.L. [1976] - Nucl. Phys., A259:365.

Pandy, M.S., Garg, J.B., Harvey, J.A. & Good, W.M. [1975] - Proc. Conf. on Nuclear Cross Sections & Technology, Washington, NBS-SPEC-PUB 425.

Sullivan, J.G., Warner, G.G., Block, R.C. & Hockenbury, R.W. [1969] - Rensselaer Polytechnic Institute unpublished report RPI-328-155.

TABLE 1

RESONANCE PARAMETERS FOR ^{54}Fe

E_n a) (keV)	$g\Gamma_\gamma\Gamma_n/\Gamma$ b) (eV)	$g\Gamma_\gamma\Gamma_n/\Gamma$ c) (eV) f)	$g\Gamma_n$ d) (eV)	ℓ e)	J e)	$g\Gamma_n$ e) (eV)
3.097	0.0030		0.0030	2		
7.68 (10)	1.8 (4)	2.5		0	$^1/_2{}^+$	1040
9.482	0.55	0.51	(2.8)		$(^3/_2)$	1.2
11.18	0.69	0.80 (16)				7.7
13.58	0.034		0.035	2		
14.46	0.62	0.53 0.92 (16)	(1.8)		$(^3/_2)$	1.4
19.26	0.047		0.049	2		
23.01	0.39	0.57 (11)	(0.7)		$(^1/_2)$	
28.19	0.17	0.16 (6)	(0.5)		$(^1/_2)$	
30.64	0.96	1.07 (16)				7.7
[34.21 ^{56}Fe	0.015 (2)]					
35.21	0.26	0.33 (7)	(0.5)		$(^1/_2)$	
38.39	0.92	1.00 (15)	(1.4)		$(^1/_2)$	
39.09	0.82	1.31 (19)				17
41.15	0.028			2		
50.09	0.075			2		
51.52	0.36	0.40 (8)	(0.6)		$(^1/_2)$	6
52.62	2.40 (40)	1.8 (3)		0	$^1/_2{}^+$	1950
53.54	0.60	0.76 (11)				17
55.0	0.68		(1.3)		$(^1/_2)$	
55.35	0.68	0.90 (13)				32
59.3		0.46 (8)				
63.45	0.012 (8)		0.012	2		
68.67	0.31	0.5 (1)	(4)			
71.75	1.32 (26)	0.8 (2)		0	$^1/_2{}^+$	1540
75.70	0.76	1.0 (2)	(4)			
77.12	1.62	1.5 (3)	(8)		$(^3/_2)$	4

TABLE 1 (Cont'd)

E_n [a] (keV)	$g\Gamma_\gamma\Gamma_n/\Gamma$ [b] (eV)	$g\Gamma_\gamma\Gamma_n/\Gamma$ [f] (eV)	$g\Gamma_n$ [d] (eV)	ℓ [e]	J [e]	$g\Gamma_n$ [e] (eV)
81.17	0.30 (3)		(4)			
83.08	1.27		(8)		$(3/2)$	
83.35	0.45 (3)	~1.7	(8)		$(3/2)$	
87.20	0.50	0.8 (2)	(14)		$(3/2)$	
97.65	0.24 (3)		(20)		$(3/2)$	
98.61	1.65 (25)	3.2 (5)		0	$1/2^+$	550
99.70	0.79		(10)			
Thick Target Results						
101.6	0.35 (2)		(10)			
104.1	0.79	1.1 (2)	(10)			
112.5	0.72		(10)			
112.8	0.56	1.5 (3)	(10)			
115.7	1.21	1.3 (2)				26
119.7	1.11					26
120.6	0.89	2.6 (4)				40
126.2	2.59	2.3 (3)				60
130.1	3.22 (64)	3.0 (6)		0	$1/2^+$	3340
135.5	0.69					80
137.7	0.96		(30)			
140.8	0.48		(10)			
142.6	1.72		(10)			
145.3	0.56		(40)			
147.8	2.31 (46)	3.0 (6)		0	$1/2^+$	3380
150.2	2.88		(30)			
152.5	1.78		(30)			
153.0	1.14					60
156.9	1.45		(30)			
159.0	1.89	3.9 (8)				100

TABLE 1 (Cont'd)

E_n [a] (keV)	$g\Gamma_\gamma\Gamma_n/\Gamma$ [b] (eV)	$g\Gamma_\gamma\Gamma_n/\Gamma$ [f] (eV)	$g\Gamma_n$ [d] (eV)	ℓ [e]	J [e]	$g\Gamma_n$ [e] (eV)
164.4	4.12					105
165.1	0.81					75
173.7	0.82		80 (40)			
174.0	3.5 (11)	2.4 (5)		0	$^1/_2^+$	3680
177.7	1.88		(10)			
182.0	1.20					150
188.7	0.49 (3)		(40)			
191.7	1.33		(40)			
192.2	10.0 (40)			0	$^1/_2^+$	40000
193.7	1.14		(40)			
194.2	1.69					100
197.3	1.23		(40)			
203.6	2.37					25
206.5	1.87		90 (30)			
207.2	1.32		(40)			
209.5	1.54					60
213.5	2.09		100 (40)			
215.8	0.44					
222.4	0.54 (4)					
223.3	1.70					
223.5	1.50 (30)			0	$^1/_2^+$	730
225.3	2.66					
227.6	1.51					
228.8	1.64					
230.7	2.56		200 (50)			450
233.2	1.91					
237.2	2.35					
241.5	1.46					

TABLE 1 (Cont'd)

E_n [a] (keV)	$g\Gamma_\gamma\Gamma_n/\Gamma$ [b] (eV)	$g\Gamma_\gamma\Gamma_n/\Gamma$ [f] (eV)	$g\Gamma_n$ [d] (eV)	ℓ [e]	J [e]	$g\Gamma_n$ [e] (eV)
244.7	1.82					720
246.8	5.7 (14)			0	$^1/_2^+$	19700
252.0	1.24					
254.3	1.56					
256.7	1.19 (8)					
258.0	-			0	$^1/_2^+$	3360
261.8	2.28					
262.6	3.23					
263.6	2.30					
266.3	0.79					
270.0	1.05					
270.9	1.50					
275.8	1.43 (10)		300 (100)			
276.7	4.37		100 (100)			300
279.5	0.66 (5)					
280.4	0.64					150
282.3	1.91 (17)					
288.7	2.02					
291.1	1.1 (2)			0	$^1/_2^+$	1100
291.7	0.99 (20)					
292.3	0.98					
302.8	1.26					
305.2	3.21					190
308.1	2.7 (8)			0	$^1/_2^+$	5400
308.4	2.39 (19)					
311.0	1.79					
315.5	0.84 (5)					

TABLE 1 (Cont'd)

E_n [a] (keV)	$g\Gamma_\gamma\Gamma_n/\Gamma$ [b] (eV)	$g\Gamma_\gamma\Gamma_n/\Gamma$ [f] (eV)	$g\Gamma_n$ [d] (eV)	ℓ [e]	J [e]	$g\Gamma_n$ [e] (eV)
321.3	3.11		400 (100)			200
323.5	3.90		300 (100)			100
325.3	2.86					
326.3	6.0 (30)			0	$^1/_2^+$	20000
329.5	0.65					
331.9	1.94					
332.4	3.6 (18)			0	$^1/_2^+$	24000
335.8	2.03 (20)					
338.6	1.40 (14)					
343.0	2.76		300 (100)			
344.4	1.64					250
356.3	5.18					350
360.1	2.32					
362.8	0.59 (6)					230
367.4	7.06					400
369.3	2.04 (24)		400 (100)			
371.0	2.10 (32)			0	$^1/_2^+$	9400
374.0	1.37		400 (100)			
382.0	2.71 (27)		450 (120)			450
383.8	0.81 (14)					
390.0	4.71					100
395.6	0.86		300 (100)			
396.5	1.65					
397.6	1.83					
401.7	2.67 (16)					300
404.9	1.34					
405.6	1.30					
408.3	2.35		300 (100)			
411.4	2.42					

TABLE 1 (Continued)

E_n [a] (keV)	$g\Gamma_\gamma\Gamma_n/\Gamma$ [b] (eV)	$g\Gamma_\gamma\Gamma_n/\Gamma$ [f] (eV)	$g\Gamma_n$ [d] (eV)	ℓ [e]	J [e]	$g\Gamma_n$ [e] (eV)
412.1	1.68					
414.1	3.7 (15)			0	$^1/_2^+$	26400
415.3	3.91					
416.2	-					1000
420.9	0.65 (10)		(500)			
426.0	2.6 (10)			0	$^1/_2^+$	8400
426.8	1.56 (12)					
429.0	0.77 (8)		(500)			
431.0	5.10					650
433.0	3.6 (14)			0	$^1/_2^+$	32000
441.7	7.48					600
445.3	9.24					875
451.2	1.80 (10)					
453.3	2.0 (6)			0	$^1/_2^+$	3000
457.6	2.20 (15)					
464.0	2.01 (23)					
467.3	4.00					
468.8	4.42					360
472.6	1.28 (17)					450
474.8	1.41 (15)					
477.3	2.81					
480.0	2.18 (15)					
484.0	3.06					
487.5	3.2 (13)			0	$^1/_2^+$	15400
488.5	1.21 (18)					650
493.1	2.69 (22)					
496.6	2.31 (23)					

TABLE 1 (Cont'd)

a) Systematic error ±0.1%. The energies of the s-wave resonances are taken from Pandy *et al.* [1975].

b) Statistical and background errors are less than 5% unless the error in the last significant figure is quoted in parentheses [*e.g.* 2.10 (110) ≡ 2.10 ± 1.10]. Normalisation errors of from 3 to 10% are not included.

c) From Hockenbury *et al.* [1969].

d) $g\Gamma_n$ used for self-shielding and multiple scattering correction is the total cross section value Pandy *et al.* [1975] unless noted. Assumed values are given in parentheses. Above 200 keV $g\Gamma_n$ = 100 eV is assumed. When $\Gamma_n << \Gamma_\gamma$, Γ_γ = 1.0 eV is assumed.

e) s-wave and $g\Gamma_n$ values from Pandy *et al.* [1975]. d-wave and probable J^π assignments from this analysis.

f) From Beer & Spencer [1975].

TABLE 2

AVERAGE RESONANCE PARAMETERS

ℓ	0	1	1+2	(2)
E_{max} (keV)	<500	<100	<500	300-400
$D(\ell)$ (keV)	22±4[a]	4.6	3.2	
$\Gamma_\gamma(\ell)$	3.2	0.45		1.20
S.D. (eV)	±2.0	±0.33		±0.6
$10^4 S_\ell$	8.6[b]			
S.D.	±2.6			
N	20	22	133	27

a) Corrected for missed resonances Pandy *et al.* [1975].

b) From Pandy *et al.* [1975].

c) Derived from maximum gradient in Figure 2.

TABLE 3

AVERAGE CAPTURE CROSS SECTIONS

Energy (keV)	σ (mb)	S.D. (mb)
3- 4	4.51	0.26
7- 8	1160.0	300
9- 10	245.0	12
10- 20	46.6	2.3
20- 30	9.8	0.5
30- 40	35.7	1.8
40- 50	0.29	0.02
50- 60	38.2	2.1
60- 70	2.0	0.12
70- 80	21.0	1.2
80- 90	12.7	0.7
90-100	11.5	0.9
100-150	12.3	1.7
150-200	18.2	2.4
200-250	12.7	1.0
250-300	9.1	0.9
300-350	11.8	1.5
350-400	7.5	0.4
400-450	9.8	1.1
450-500	6.6	0.7

Maxwellian averaged capture cross section at 30 keV

$$\frac{\langle \sigma \cdot v \rangle}{v_T} = 33.6 \pm 2.7 \text{ mb}$$

Resonance component of resonance integral above 2.5 keV

$$\Sigma A_\gamma / E = 262.0 \pm 40.0 \text{ mb}$$

TABLE 4

s-WAVE VALENCE PARAMETERS

E_λ (keV)	$\Gamma^0_{\lambda n}$ (eV)	Q_λ	$\Gamma^V_{\lambda\gamma}$ (eV)	$\Gamma_{\lambda\gamma}$ (eV)
7.68	11.9	0.171	2.0	1.8
52.9	8.48	0.152	1.3	2.4
71.75	5.75	0.149	0.86	1.3
98.66	1.75	0.139	0.24	1.6
130.1	9.26	0.128	1.2	3.2
147.8	8.79	0.122	1.1	2.3
174.0	8.82	0.119	1.1	3.5
192.2	91.2	0.111	10.1	10.0
223.5	1.54	0.103	0.16	1.5
246.8	39.7	0.095	3.8	5.7
258.0		not observed		
291.1	2.04	0.084	0.17	1.1
308.1	9.73	0.080	0.78	2.7
326.3	35.0	0.075	2.6	6.0
332.4	41.6	0.073	3.0	3.6
371.0	15.4	0.064	0.99	2.1
414.1	41.0	0.052	2.1	3.7
426.0	12.9	0.054	0.70	2.6
433.0	48.6	0.051	2.5	3.6
453.3	4.46	0.048	0.21	2.0
487.5	22.1	0.043	0.95	3.2
			$\bar{\Gamma}^V_\gamma = 1.83$	$\bar{\Gamma}_\gamma = 3.2$

N=11 $\rho_I(<300) = 0.97$ $\langle\Gamma_\gamma\rangle = 3.2\pm2.5$

N=15 $\rho_I(<400) = 0.94$ $\langle\Gamma_\gamma\rangle = 3.3\pm2.3$

N=20 $\rho_I(<500) = 0.90$ $\langle\Gamma_\gamma\rangle = 3.2\pm2.0$

TABLE 5

FINAL STATE $\ell_n = 1$ SPECTROSCOPIC DATA

E_μ (MeV)	J_μ^{π} a)	$10^4 \times q_\mu$	S_μ a)	$\Gamma_{\gamma\mu}^V$ (meV)	$\Gamma_{\gamma\mu}$ (meV)
0.00	$^3/_2^-$	7.82	0.73	1260	1390
0.41	$^1/_2^-$	4.18	0.59	476	258
1.93	$^1/_2^-$	4.18	0.07	33	2
2.06	$^3/_2^-$	7.82	0.08	65	42
2.48	$^3/_2^-$	7.82	0.15	101	40
3.04	$^3/_2^-$	7.82	0.03	17	67
3.56	$^3/_2^-$	7.82	0.11	44	48
3.80	$^1/_2^-$	4.18	0.50	90	50
5.78	$^1/_2^-$	4.18	0.04	2	21

a) Taken from Kocher & Haeberli [1972]

b) Thermal partial widths derived from Arnell [1967] assuming Γ_γ = 2.1 eV for the 7.7 keV resonance

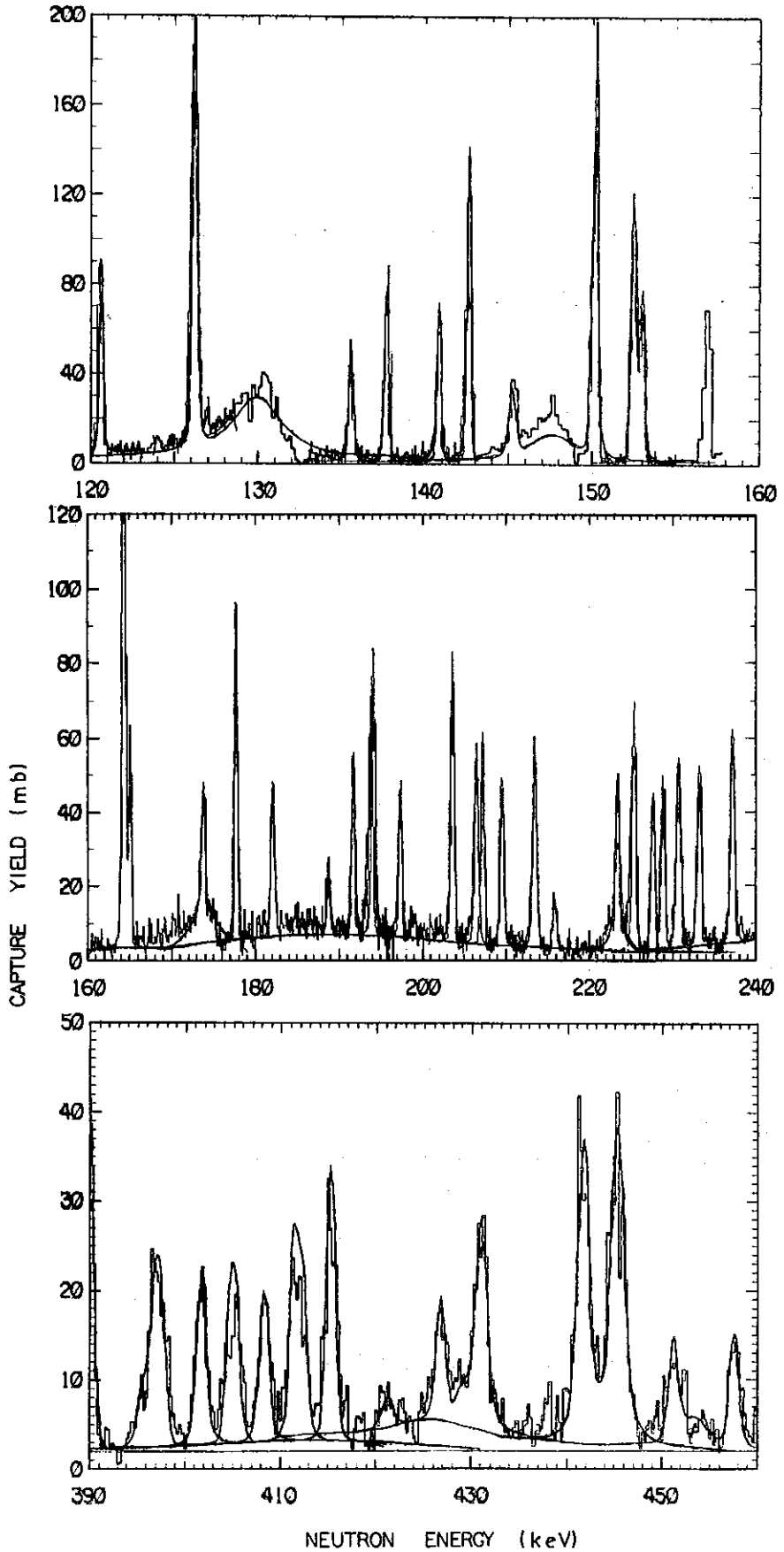

FIGURE 1. CAPTURE YIELDS (mb) AT THE s-WAVE RESONANCES

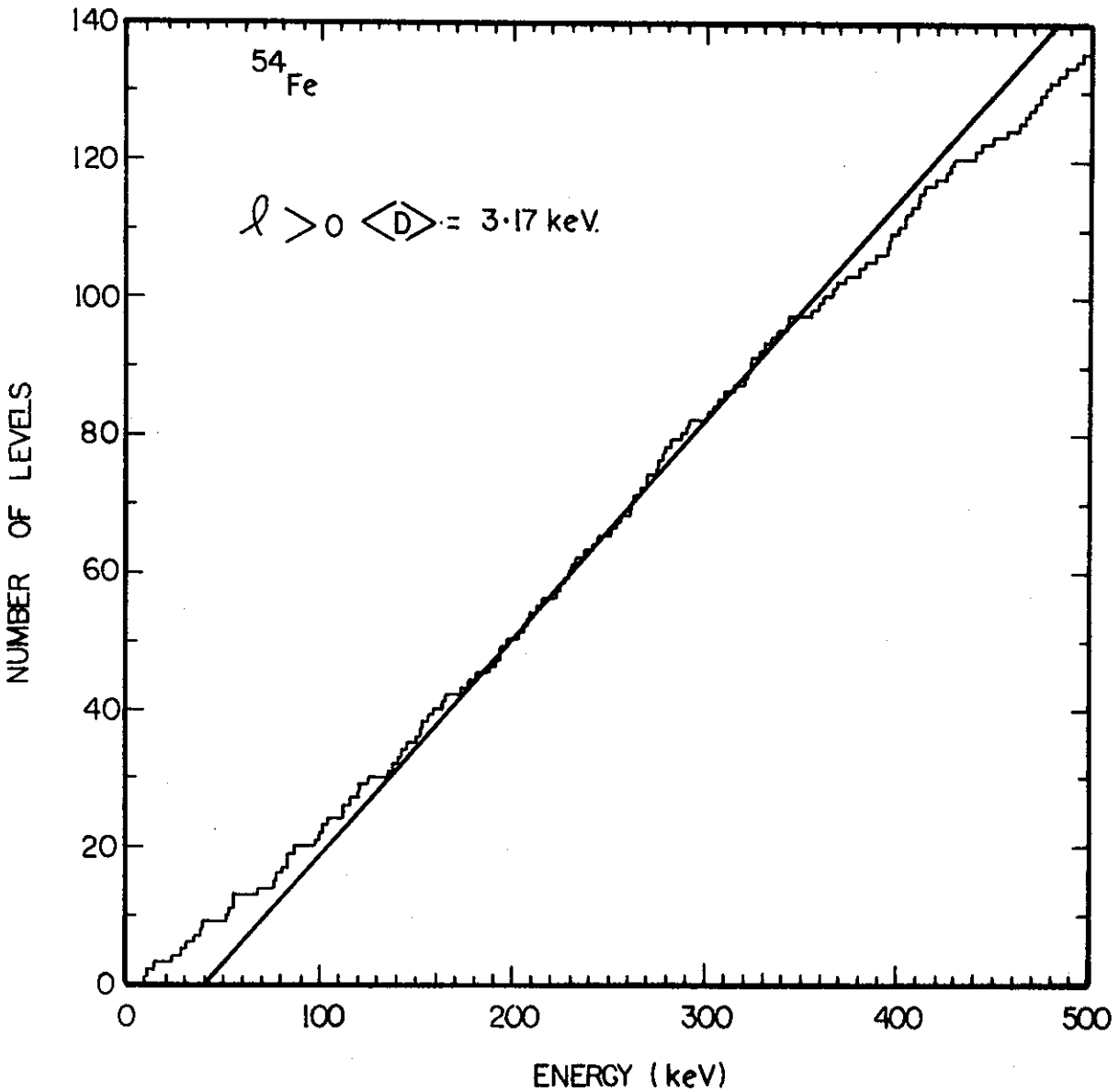

FIGURE 2. ℓ>0 LEVEL DENSITY

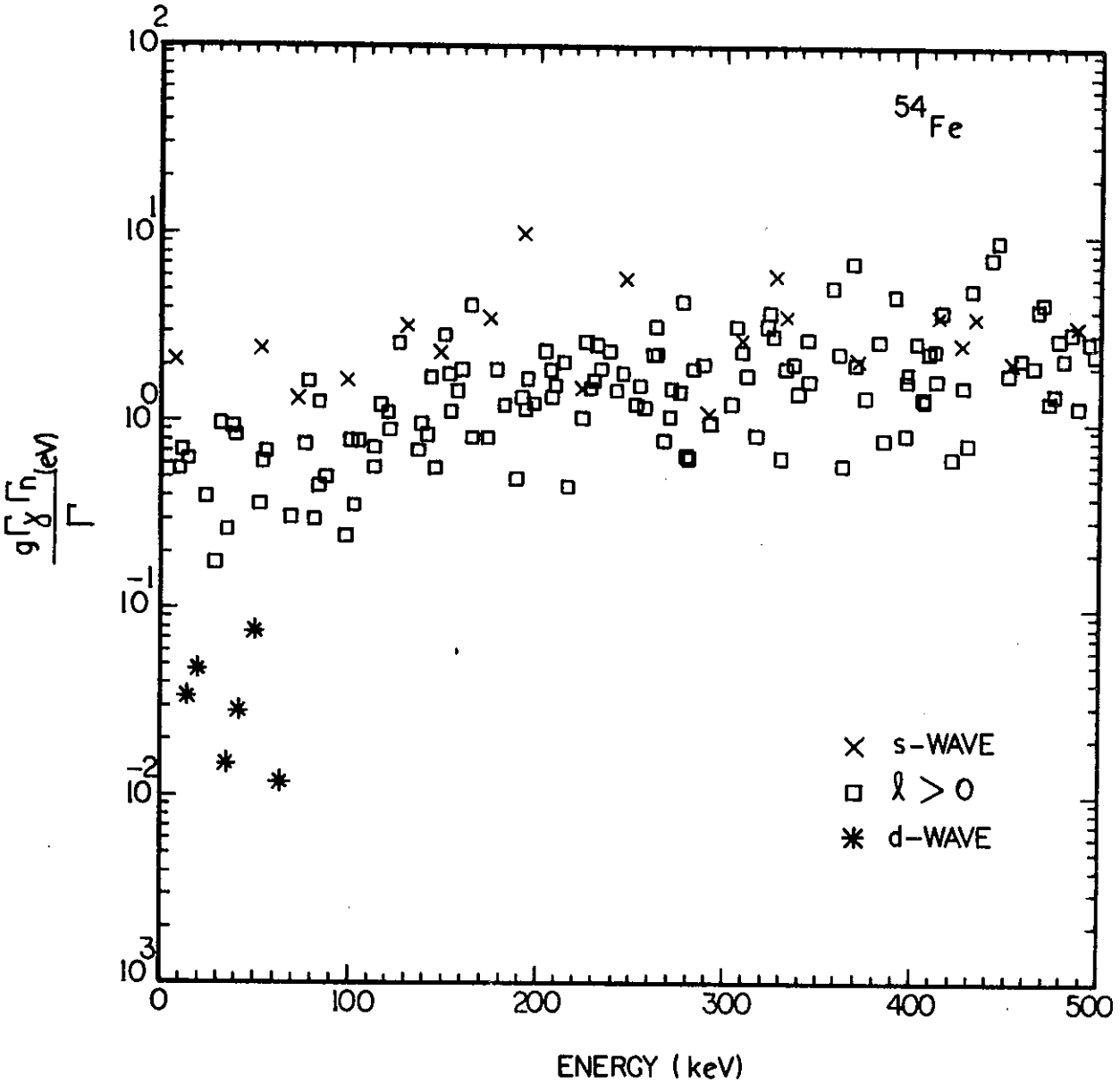

FIGURE 3. VARIATION OF $g\Gamma_\gamma\Gamma_n/\Gamma$ WITH ENERGY

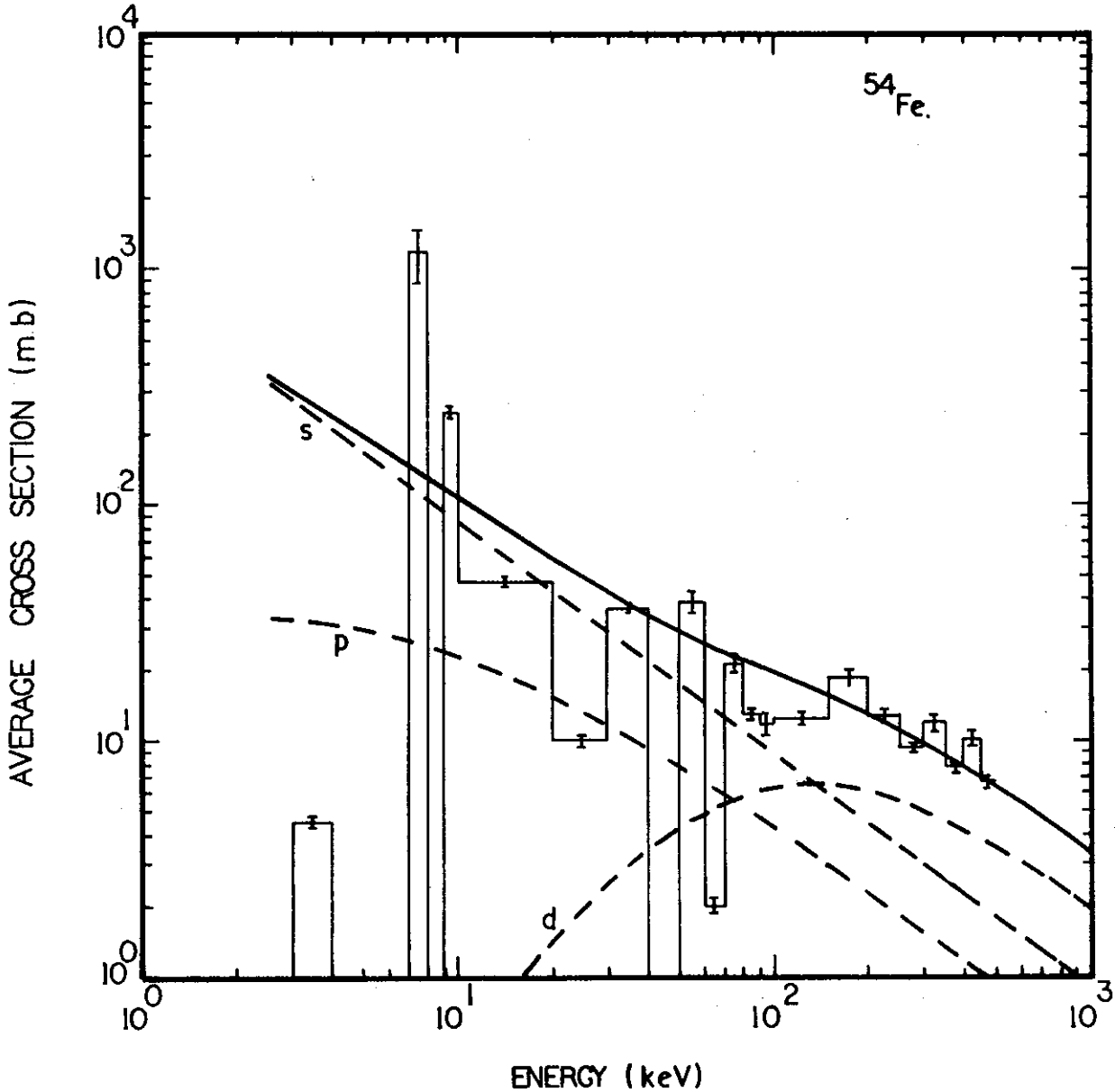

FIGURE 4. COMPARISON OF AVERAGED DATA WITH CALCULATED CROSS SECTIONS

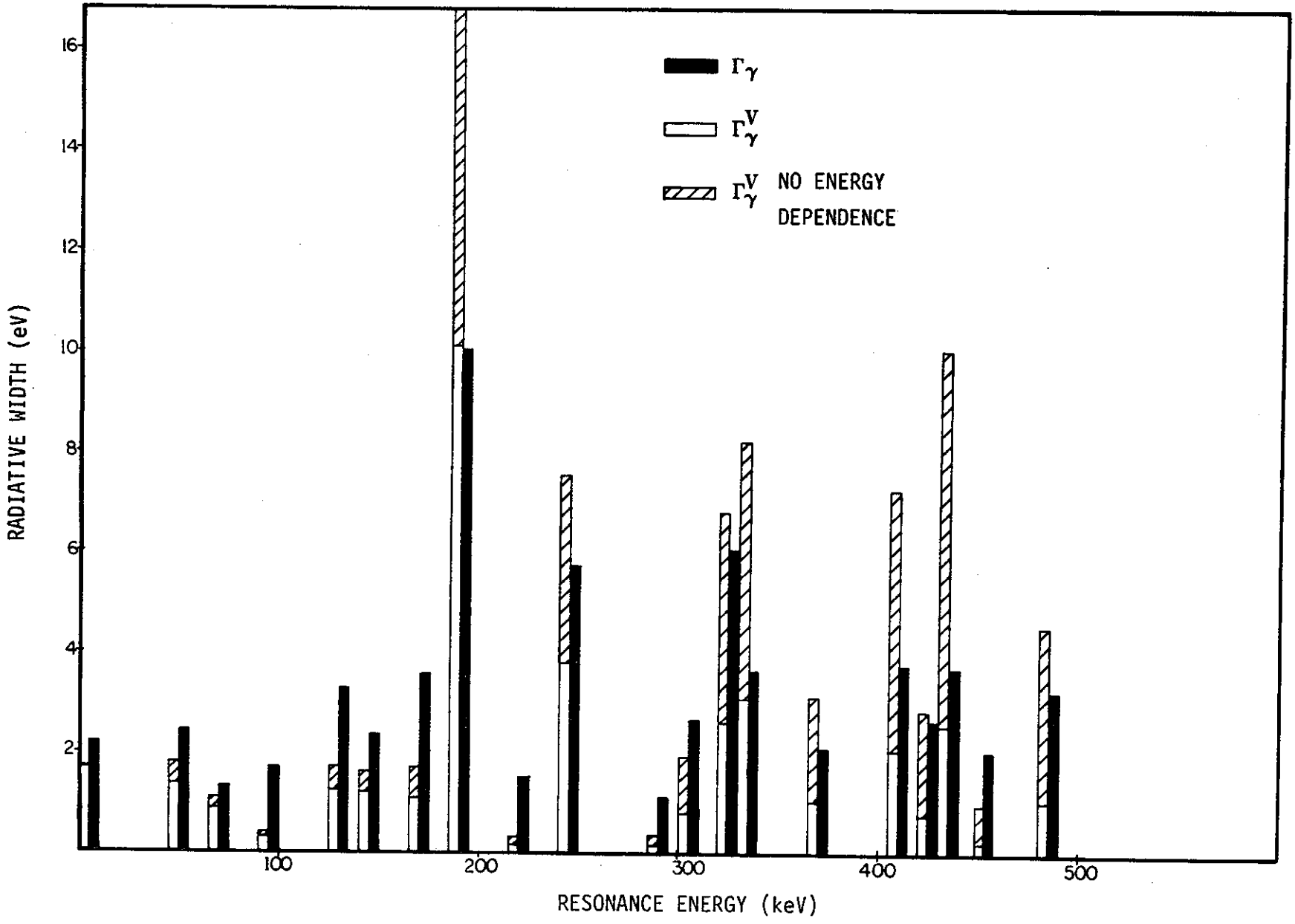

FIGURE 5. ENERGY DEPENDENCE OF MEASURED AND VALENCE s-WAVE WIDTHS